Model reference adaptive switching control of a linearized hypersonic flight vehicle model with actuator saturation

C Dong, Y Hou*, **Y Zhang,** and **Q Wang**
Beijing University of Aeronautics and Astronautics, Beijing, People's Republic of China

The manuscript was received on 13 June 2009 and was accepted after revision for publication on 26 January 2010.

DOI: 10.1243/09596518JSCE829

Abstract: In order to address the control of an air-breathing hypersonic flight vehicle (AHFV) with actuator saturation, a model reference adaptive switching control (MRASC) approach is proposed. The design of the MRASC system is centred around a linearized longitudinal-motion flexible model at a Mach 8, altitude of 10 000 ft, and dynamic pressure of 1017 lb/ft^2 flight condition. A switched reference system (SRS) is established to describe the desired dynamics of the AHFV with/without actuator saturation, and correspondingly, a switched adaptive controller (SAC) is constructed utilizing the hyperstability method. By switching between the subsystems of the SRS and the corresponding subcontrollers of the SAC, the MRASC system achieves the desired performance and is globally asymptotically stable under limited disturbances, provided that a simple linear-matrix-inequality-based sufficient condition holds. Although it is too early to say that the proposed scheme gives desired anti-saturation performance with respect to large disturbances, within a large flight envelope, there are still some advantages that will improve performance.

Keywords: hypersonic flight vehicles, actuator saturation, switched systems, adaptive control, switching control

1 INTRODUCTION

The development of a hypersonic flight vehicle will create new opportunities in low-orbit space flight, high-speed civilian transportation, and military operations [**1–4**]. However, after four decades of research, there still exist many challenging and interesting problems. One such issue is flight controller design.

The complex dynamics of an air-breathing hypersonic flight vehicle (AHFV) that are the result of high dynamic pressures, high acceleration load, and constantly changing flight environment, mean that designing a reliable and effective controller is a difficult task. Classical proportional–derivative (PD) controllers with large time-varying gains may guarantee a satisfactory performance. However, large gains would inevitably induce high noise amplification and high cost of control [**2**]. Robust controllers designed by the H_∞ control or μ synthesis methods may achieve the desired performance when controlling the AHFV. However, the H_∞ control method is essentially an optimal control method for worst-case situations, hence the controllers are deemed to be conservative when compared with PD controllers [**3**, **4**]. Although the μ synthesis method may obtain less conservative results, it is computationally infeasible for high-order plants [**2**]. Thus, it is necessary to investigate an alternative method for the control of an AHFV.

The model reference adaptive control (MRAC) strategy, whose controller parameters are adjusted by means of minimizing the differences between the reference model output and the plant output, is less sensitive to changes in the environment, modelling errors, and non-linearities within the system. There has been considerable research effort in this area in recent years and the number of applications using

**Corresponding author: Beijing University of Aeronautics and Astronautics, Beijing 100191, People's Republic of China.*
email: egibus@163.com

this methodology is steadily increasing. Mooij [2] has shown that a classical MRAC scheme is a promising control methodology for application to hypersonic aircraft.

However, actuator saturation, which can occur in many practical systems, must be considered because it will lead to performance degradation and even instability. Generally speaking, there are two approaches to addressing actuator saturation. One approach is the use of the anti-windup scheme in which an additional feedback is introduced to avoid saturation. Most anti-windup-based schemes are only applicable to open-loop stable systems. For open-loop unstable systems (apparently, the AHFV is strictly unstable at most operating points), few results are available, especially for uncertain unstable systems [5]. The other possible approach to addressing the saturation problem is to consider it to be a constraint from the beginning of the design process. Although this approach (the so-called direct approach) is appealing, the designed controllers are conservative because actuator saturation is encountered only rarely or temporarily in practice [6].

In this paper a model reference adaptive switching control (MRASC) strategy, which is an extension of the classical MRAC methodology, is proposed as an approach to the design of a controller with actuator saturation for an AHFV. A switched reference system is established to describe the desired dynamics of the AHFV with/without actuator saturation. Correspondingly, based on the hyperstability method [7], a switched adaptive controller composed of finite adaptive controllers is designed. During the control process, one subsystem in the switched reference system and its corresponding adaptive controller are activated together to prevent actuator saturation, according to a switching signal generated by decision variables (such as the events that may induce the actuator saturation). Considering that the closed-loop system is a switched non-linear system [8], stability analysis of the control scheme is proved by the multiple Lyapunov functions method [9] and the Lure–Postnikov Lyapunov function [10].

Main contributions of this study are as follows.

1. The proposed MRASC strategy is applied to control the AHFV with actuator saturation. This strategy can improve the performance, and ensure globally asymptotical stability provided that a linear matrix inequality (LMI)-based sufficient condition is satisfied.
2. Contrary to most anti-windup schemes, the proposed scheme does not need the precondition of an open-loop system being stable and allows systems to be disturbed to some extent. In addition, because the subsystem of the switched reference system and its corresponding adaptive controller are activated only when saturation arises or probably arises, a less conservative controller is achieved as compared to direct approaches.

The remainder of this paper is organized as follows. Section 2 illustrates the linearized flexible model of the AHFV and the architecture of the MRASC scheme. Section 3 performs the stability analysis. The proposed scheme is numerically validated in section 4. Finally, conclusions are presented in section 5.

Notation

The notation in this study is standard. $\Re^+$ denotes the set of real numbers. $\Re^n$ stands for the set of real vectors. The transpose and the inverse of a real matrix $\mathbf{M}$ are $\mathbf{M}^{\mathrm{T}}$ and $\mathbf{M}^{-1}$, respectively. $\mathbf{M}>0(\mathbf{M}\geqslant 0)$ indicates that the real matrix $\mathbf{M}$ is positive-definite (semi-positive definite), and $\mathbf{M}<0(\mathbf{M}\leqslant 0)$ denotes a negative-definite (semi-negative definite) matrix. $\mathbf{I}$ denotes the identity matrix and diag($*$) stands for a diagonal matrix. For every $\boldsymbol{p}=(p_1,p_2,\cdots,p_n)\in\Re^n$, let $\|\boldsymbol{p}\|_1=\sum_{i=1}^{n}|p_i|$ represent the 1-norm, $\|\boldsymbol{p}\|=(\boldsymbol{p}^{\mathrm{T}}\boldsymbol{p})^{1/2}$ denote the Euclidean norm of $\boldsymbol{p}$ and $\mathrm{sgn}\,(\boldsymbol{p})$ represent the signum function.

2 THE MRASC METHOD

2.1 Mathematical model of the AHFV

The hypersonic vehicle considered in this study is the same as that of [11] where a generic hypersonic vehicle that is similar to the X-30 is considered. In the model, one elastic degree of freedom is included. The linearized longitudinal dynamical model described in the state space is given in equation (1), referenced to a flight condition of Mach 8, an altitude of 10 000 ft, and a dynamic pressure of 1017 lb/ft^2.

$$\dot{\boldsymbol{x}}(t)=\mathbf{A}\boldsymbol{x}(t)+\mathbf{B}(\boldsymbol{u}(t)+\boldsymbol{d}(t)) \tag{1}$$

where $\mathbf{A}$ and $\mathbf{B}$ are the system and input matrices, respectively. Detailed expressions for them can be found in [12] and hence they are omitted here. $\boldsymbol{d}(t)$ represents disturbances, and is bounded by a known function $\delta(t)$ such that $\|\boldsymbol{d}(t)\|\leqslant\delta(t)$.

The state variable $\boldsymbol{x}\in\Re^7$ and the input $\boldsymbol{u}\in\Re^3$ utilized in this model are given by

$$\boldsymbol{x} = [h\ (\text{ft}) \quad V\ (\text{ft/s}) \quad \alpha\ (\text{rad}) \quad \theta\ (\text{rad}) \\ q\ (\text{rad/s}) \quad \eta\ (\text{-}) \quad \dot{\eta}\ (1/\text{s})]^{\mathrm{T}}$$

$$\boldsymbol{u} = [\delta_{\mathrm{e}}\ (\text{rad}) \quad A_{\mathrm{d}}\ (\text{-}) \quad \dot{m}_{\mathrm{f}}\ (\text{slug/s})]^{\mathrm{T}}$$

where h stands for the altitude, V represents the vehicle flight velocity, α is the angle of attack, θ denotes the pitch attitude, q is the pitch rate, η denotes the generalized elastic coordinate, δ_{e} is the pitch control surface deflection, A_{d} represents the diffuser area ratio, and $\dot{m}_{\mathrm{f}}$ denotes the fuel mass flowrate.

The input trim condition for the pitch control surface deflection δ_{e} and the diffuser area ratio A_{d} are 0.52 rad and 0.1482, respectively.

In this work, the control inputs δ_{e} and A_{d} are constrained to vary within the range $[-1.14, 0.087]$ and $[-0.148, 0.85]$, respectively, because δ_{e} should remain within the range $[-0.61, 0.61]$ and A_{d} can only vary within $[0, 1]$ in practice.

2.2 Architecture of the MRASC scheme

The MRASC scheme for the AHFV is described in Fig. 1. In the scheme, the switched reference system describes the desired dynamics of the AHFV with/without actuator saturation. One subsystem (denoted by S1) of the switched reference system (SRS) describes the dynamics without actuator saturation, whereas other subsystems (denoted by S2) specify the desired dynamics for the case of actuator saturation and the cases where the actuator is prone to saturation. Correspondingly, a switched adaptive controller is designed to make the system dynamics track the desired dynamics. During the control process, one subsystem in S2 and its corresponding controller are activated together to prevent actuator saturation, according to a switching signal generated by decision variables (such as control input amplitude or events that may induce the actuator saturation), whereas at other times S1 and its corresponding controller are active in the system.

The reference input of the SRS is generated by a linear quadratic regulator. The regulator is used to minimize the difference between $\boldsymbol{x}_{\mathrm{m}}(t)$ and the command signal $\boldsymbol{c}(t) = [h_{\mathrm{c}}, V_{\mathrm{c}}, \alpha_{\mathrm{c}}, \theta_{\mathrm{c}}, q_{\mathrm{c}}, \eta_{\mathrm{c}}, \dot{\eta}_{\mathrm{c}}]^{\mathrm{T}}$. This is similar to the approach of [**13**]. The detailed structures of the SRS, switched adaptive controller (SAC), and linear quadratic regulator are illustrated in the following discussions.

SRS

$$\dot{\boldsymbol{x}}_{\mathrm{m}}(t) = \mathbf{A}_{\mathrm{m}_\sigma}\boldsymbol{x}_{\mathrm{m}}(t) + \mathbf{B}_{\mathrm{m}_\sigma}\boldsymbol{r}(t) \tag{2}$$

where $\boldsymbol{x}_{\mathrm{m}} \in \Re^7$ is the reference state and $\boldsymbol{r} \in \Re^3$ is the reference input, $\sigma(t, \psi) : [0, +\infty) \otimes \boldsymbol{\Psi} \rightarrow \boldsymbol{\Omega} = \{1, 2, \cdots, N\}$ is the piecewise constant switching signal taking value from a finite index set $\boldsymbol{\Omega}$, and is continuous from the right everywhere. $\psi \in \boldsymbol{\Psi}$ is the decision variable and $\boldsymbol{\Psi}$ is the decision variable set. For any $i \in \boldsymbol{\Omega}$, $(\mathbf{A}_{\mathrm{m}_i}, \mathbf{B}_{\mathrm{m}_i})$ is the subsystem of the SRS, that

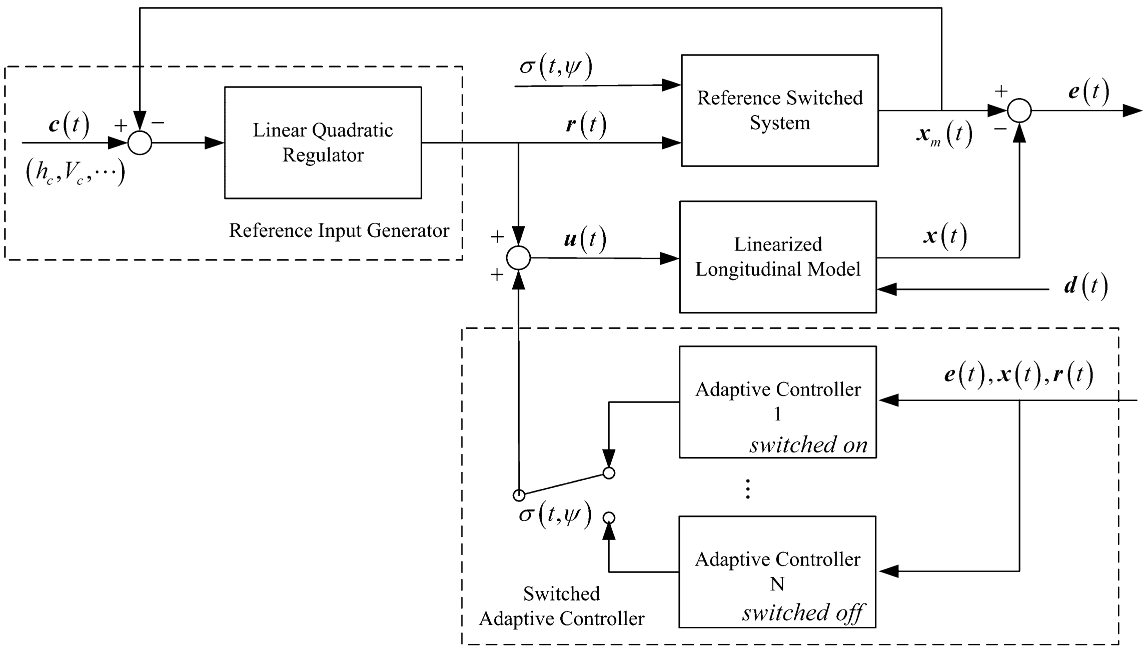

Fig. 1 Architecture of the model reference adaptive switching control scheme

satisfies the following condition of the Erzberger perfect model so as to ensure the desired steady accuracy [**14**], and $\mathbf{A}_{\mathrm{m}_i}$ is Hurwitz stable.

SAC

Define the state error as equation (3)

$$\boldsymbol{e}(t) = \boldsymbol{x}_{\mathrm{m}}(t) - \boldsymbol{x}(t) \tag{3}$$

then the SAC can be written as

$$\boldsymbol{u}(t) = \boldsymbol{r}(t) + \mathbf{F}_{\sigma}(t)\boldsymbol{x}(t) + \mathbf{G}_{\sigma}(t)\boldsymbol{r}(t) + \delta(t)\,\mathrm{sgn}\left(\mathbf{B}^{\mathrm{T}}\mathbf{P}\boldsymbol{e}(t)\right)$$

$$\mathbf{F}_i(t) = \begin{cases} \int_0^t \mathbf{K}\mathbf{B}^{\mathrm{T}}\mathbf{P}\boldsymbol{e}(\tau)\boldsymbol{x}^{\mathrm{T}}(\tau)\mathrm{d}\tau + \boldsymbol{\alpha}_i\mathbf{B}^{\mathrm{T}}\mathbf{P}\boldsymbol{e}(t)\boldsymbol{x}^{\mathrm{T}}(t) + \mathbf{F}_i\left(t_i^0\right), \\ \text{if } \sigma(t,\psi) = i \\ \int_0^t \mathbf{K}\mathbf{B}^{\mathrm{T}}\mathbf{P}\boldsymbol{e}(\tau)\boldsymbol{x}^{\mathrm{T}}(\tau)\mathrm{d}\tau + \mathbf{F}_i\left(t_i^0\right), \\ \text{if } \sigma(t,\psi) \neq i \end{cases}$$

$$\mathbf{G}_i(t) = \begin{cases} \int_0^t \mathbf{L}\mathbf{B}^{\mathrm{T}}\mathbf{P}\boldsymbol{e}(\tau)\boldsymbol{r}^{\mathrm{T}}(\tau)\mathrm{d}\tau + \boldsymbol{\beta}_i\mathbf{B}^{\mathrm{T}}\mathbf{P}\boldsymbol{e}(t)\boldsymbol{r}^{\mathrm{T}}(t) + \mathbf{G}_i\left(t_i^0\right), \\ \text{if } \sigma(t,\psi) = i \\ \int_0^t \mathbf{L}\mathbf{B}^{\mathrm{T}}\mathbf{P}\boldsymbol{e}(\tau)\boldsymbol{r}^{\mathrm{T}}(\tau)\mathrm{d}\tau + \mathbf{G}_i\left(t_i^0\right), \\ \text{if } \sigma(t,\psi) \neq i \end{cases} \tag{4}$$

where $\mathbf{F}_i(t)$ and $\mathbf{G}_i(t)$ are the feedback controller and the feedforward controller, respectively, $\mathbf{P} > 0$ satisfies an LMI condition for stability of the MRASC scheme, which is stated in section 3 in detail, t_i^0 represents the time at which the ith subsystem is activated for the first time, $\boldsymbol{\alpha}_i \geqslant 0, \boldsymbol{\beta}_i \geqslant 0$ are arbitrary appropriately dimensional semi-positive definite matrices, $\mathbf{K} > 0$, $\mathbf{L} > 0$ are arbitrary appropriately dimensional positive-definite matrices, and $\mathbf{F}_i\left(t_i^0\right), \mathbf{G}_i\left(t_i^0\right)$ are the initial gains satisfying $\mathbf{A}_{\mathrm{m}_i} - \mathbf{A} = \mathbf{B}\mathbf{F}_i(t_i^0)$, $\mathbf{B}_{\mathrm{m}_i} - \mathbf{B} = \mathbf{B}\mathbf{G}_i(t_i^0)$.

Remark 1

In equation (4), the proportion parts in $\mathbf{F}_i(t)$ and $\mathbf{G}_i(t)$ are set to zero when $\sigma(t,\psi) \neq i$ (i.e. when the ith subsystem and the ith controller are 'switched off'), whereas the integral parts are still updated by certain system signals. The proportion parts in $\mathbf{F}_i(t)$ and $\mathbf{G}_i(t)$ are readjusted when the ith subsystem and the corresponding ith controller are 'switched on'. A generic evolution, taking the feedback adaptive controller $\mathbf{F}_i(t)$ for example, is depicted in Fig. 2.

Remark 2

In the SAC, a non-smooth non-linear term $\delta(t)\,\mathrm{sgn}\left(\mathbf{B}^{\mathrm{T}}\mathbf{P}\boldsymbol{e}(t)\right)$ is introduced to attenuate the disturbances $\boldsymbol{d}(t)$. This idea goes back to the early work on controlling linear uncertain unstable plants with actuator saturation reported in [**5**], where a satisfactory performance was achieved by choice of a suitable time-varying sliding surface.

Remark 3

It is worth noting that the SAC is designed with respect to a known disturbance bound. This may predictably affect the performance when the actual disturbance is noticeably lower in magnitude than the bound. Hence, an accurate disturbance bound will be of great benefit to a satisfactory performance.

Linear quadratic regulator

The reference input $\boldsymbol{r}(t)$ is generated by the linear quadratic regulator as follows

$$\boldsymbol{r}(t) = -\bar{\mathbf{R}}^{-1}\mathbf{B}_{\mathrm{m}}^{\mathrm{T}}\left[\bar{\mathbf{K}}\boldsymbol{x}_{\mathrm{m}}(t) - \left[\bar{\mathbf{K}}\mathbf{B}_{\mathrm{m}}\bar{\mathbf{R}}^{-1}\mathbf{B}_{\mathrm{m}}^{\mathrm{T}} - \mathbf{A}_{\mathrm{m}}^{\mathrm{T}}\right]^{-1}\bar{\mathbf{Q}}\boldsymbol{c}(t)\right], \quad \bar{\mathbf{Q}}, \bar{\mathbf{R}} > 0 \tag{5}$$

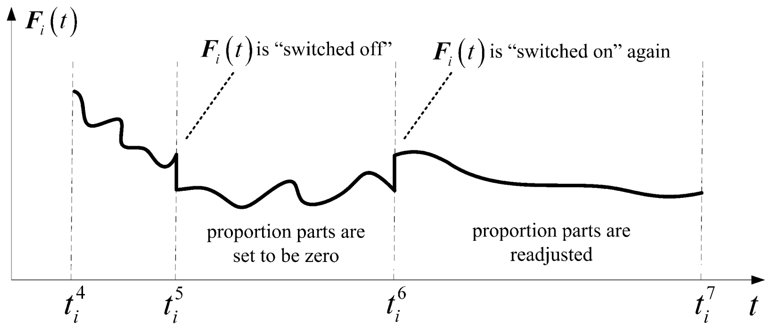

Fig. 2 A generic adaptive controller evolution

where $\mathbf{A}_\mathrm{m}$, $\mathbf{B}_\mathrm{m}$ correspond to the subsystem S1 of the SRS and $\bar{\mathbf{K}}$ is the solution of the algebraic Riccati equation

$$\mathbf{A}_\mathrm{m}^\mathrm{T}\bar{\mathbf{K}}+\bar{\mathbf{K}}\mathbf{A}_\mathrm{m}-\bar{\mathbf{K}}\mathbf{B}_\mathrm{m}\bar{\mathbf{R}}^{-1}\mathbf{B}_\mathrm{m}^\mathrm{T}\bar{\mathbf{K}}+\bar{\mathbf{Q}}=0 \tag{6}$$

This reference input $\boldsymbol{r}(t)$ can minimize the following performance index [**15**]

$$J=\frac{1}{2}\int_0^t\left[(\boldsymbol{c}(\tau)-\boldsymbol{x}_\mathrm{m}(\tau))^\mathrm{T}\bar{\mathbf{Q}}(\boldsymbol{c}(\tau)-\boldsymbol{x}_\mathrm{m}(\tau))+\boldsymbol{r}^\mathrm{T}(\tau)\bar{\mathbf{R}}\boldsymbol{r}(\tau)\right]\mathrm{d}\tau \tag{7}$$

The closed-loop switched system for the MRASC scheme can be obtained using equations (1) to (4) in the form of

$$\begin{aligned}\dot{\boldsymbol{e}}(t)=&\mathbf{A}_{\mathrm{m}_\sigma}\boldsymbol{e}(t)+[\mathbf{A}_{\mathrm{m}_\sigma}-\mathbf{A}-\mathbf{B}\mathbf{F}_\sigma(t)]\boldsymbol{x}(t)\\&+[\mathbf{B}_{\mathrm{m}_\sigma}-\mathbf{B}-\mathbf{B}\mathbf{G}_\sigma(t)]\boldsymbol{r}(t)-\mathbf{B}\boldsymbol{d}(t)\\&-\delta(t)\,\mathbf{B}\mathrm{sgn}\left(\mathbf{B}^\mathrm{T}\mathbf{P}\boldsymbol{e}(t)\right)\end{aligned} \tag{8}$$

In the rest of this study, it will be shown that if the closed-loop switched system satisfies a sufficient condition, then globally asymptotical stability as well as a satisfactory performance will be guaranteed in the presence of actuator saturation.

3 STABILITY ANALYSIS

In this section, the stability of the closed-loop switched system (8) will be proved based on the multiple Lyapunov functions method. Before performing the stability analysis, some preliminaries are given for the sake of clarity.

Lemma 1 [**9**]

Consider a family of globally asymptotically stable systems $\dot{\boldsymbol{x}}(t)=h_p(\boldsymbol{x}(t))$, where h_p, $p\in\boldsymbol{\Pi}$ are functions from $\Re^n$ to $\Re^n$ and assumed to be sufficiently regular (at least locally Lipschitz), where $\boldsymbol{\Pi}$ is a finite index set. Let V_p, $p\in\boldsymbol{\Pi}$ be a family of corresponding radially unbounded Lyapunov functions. Suppose that there exists a family of positive-definite continuous functions M_p, $p\in\boldsymbol{\Pi}$ satisfying that for every pair of switching times (t_i,t_j), $i<j$ such that $\sigma(t_i)=\sigma(t_j)=p\in\boldsymbol{\Pi}$ and $\sigma(t_k)\neq p$ for $t_i<t_k<t_j$, $V_p(\boldsymbol{x}(t_j))-V_p(\boldsymbol{x}(t_i))\leqslant -M_p(\boldsymbol{x}(t_i))$ holds. Then, the switched system $\dot{\boldsymbol{x}}(t)=h_p(\boldsymbol{x}(t))$ is globally asymptotically stable.

Lemma 2 [**9**]

Suppose that the pth subsystem is consecutively activated at the time t_i, t_j and is active during time intervals $[t_i,t_{i+1})$ and $[t_j,t_{j+1})$, $\sigma(t_k)\neq p$ for any $t_k\in(t_i,t_j)$, $V_p(\boldsymbol{x}(t_j))-V_p(\boldsymbol{x}(t_{i+1}^-))\leqslant -M_p(\boldsymbol{x}(t_{i+1}^-))$ holds. Then, the switched system $\dot{\boldsymbol{x}}(t)=h_p(\boldsymbol{x}(t))$ is globally asymptotically stable.

In this paper, Lemma 2, an extended result of Lemma 1, is used to prove the stability of the closed-loop switched system. It is easy to conclude that Lemma 2 is a special case of Lemma 1, i.e. the value of the Lyapunov function V_p when the pth subsystem is reactivated is no larger than that at which the pth subsystem was inactivated last time, which is also depicted in Fig. 3.

In the following, the stability analysis of the closed-loop switched system will be performed.

Theorem 1

If there exist positive-definite matrices $\mathbf{P}$, $\mathbf{Z}$ such that the LMI

$$\mathbf{A}_{\mathrm{m_i}}^\mathrm{T}\mathbf{P}+\mathbf{P}\mathbf{A}_{\mathrm{m_i}}+\mathbf{Z}<0 \tag{9}$$

hold for every $i\in\boldsymbol{\Omega}$, then under arbitrary switching law, the closed-loop switched system (8) is globally asymptotically stable for any bounded piecewise continuous reference input.

Proof

The proof is performed in two steps.

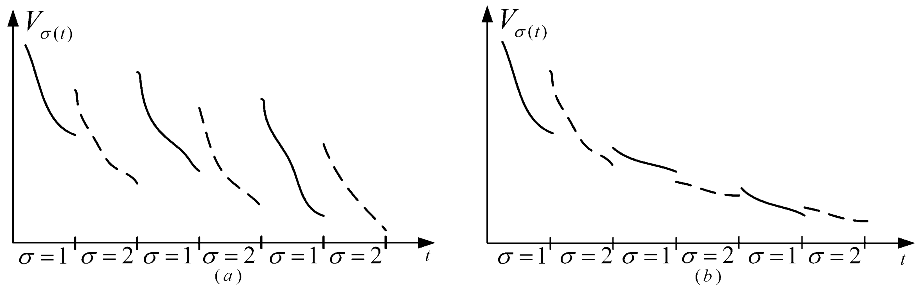

Fig. 3 Multiple Lyapunov functions method (a) for Lemma 1 and (b) for Lemma 2 (solid lines correspond to V_1, dashed lines to V_2)

First, a candidate Lure–Postnikov Lyapunov function is constructed for the closed-loop switched system, and then the globally asymptotical stability is proved for every subsystem of the closed-loop switched system. Second, the globally asymptotical stability of the closed-loop switched system is proved based on Lemma 2.

Step 1: For $\forall i \in \mathbf{\Omega}$, the following Lure–Postnikov Lyapunov function is taken for the subsystem of the closed-loop switched system

$$\begin{aligned} V_i = {} & \boldsymbol{e}^{\mathrm{T}}(t)\mathbf{P}\boldsymbol{e}(t) \\ & + 2\int_0^t \left(\mathbf{B}^{\mathrm{T}}\mathbf{P}\boldsymbol{e}(t')\right)^{\mathrm{T}} \left(\int_0^{t'} \mathbf{K}\mathbf{B}^{\mathrm{T}}\mathbf{P}\boldsymbol{e}(\tau)\boldsymbol{x}^{\mathrm{T}}(\tau)\,\mathrm{d}\tau\right)\boldsymbol{x}(t')\,\mathrm{d}t' \\ & + 2\int_{\Im(t_i^0,\, t_i^s,\, t)} \left(\mathbf{B}^{\mathrm{T}}\mathbf{P}\boldsymbol{e}(t')\right)^{\mathrm{T}} \boldsymbol{\alpha}_i \mathbf{B}^{\mathrm{T}}\mathbf{P}\boldsymbol{e}(t')\boldsymbol{x}^{\mathrm{T}}(t')\boldsymbol{x}(t')\,\mathrm{d}t' \\ & + 2\int_0^t \left(\mathbf{B}^{\mathrm{T}}\mathbf{P}\boldsymbol{e}(t')\right)^{\mathrm{T}} \left(\int_0^{t} \mathbf{L}\mathbf{B}^{\mathrm{T}}\mathbf{P}\boldsymbol{e}(\tau)\boldsymbol{r}^{\mathrm{T}}(\tau)\,\mathrm{d}\tau\right)\boldsymbol{r}(t')\,\mathrm{d}t' \\ & + 2\int_{\Im(t_i^0,\, t_i^s,\, t)} \left(\mathbf{B}^{\mathrm{T}}\mathbf{P}\boldsymbol{e}(t')\right)^{\mathrm{T}} \boldsymbol{\beta}_i \mathbf{B}^{\mathrm{T}}\mathbf{P}\boldsymbol{e}(t')\boldsymbol{r}^{\mathrm{T}}(t')\boldsymbol{r}(t')\,\mathrm{d}t' \end{aligned} \tag{10}$$

where $\Im(t_i^0, t_i^{\mathrm{s}}, t) \triangleq [t_i^0, t_i^1) \cup [t_i^2, t_i^3) \cup \cdots \cup [t_i^{\mathrm{s}}, t)$ represents the active time interval of the ith subsystem with the first and the latest being activated at t_i^0 and t_i^{s}, respectively; $t_i^2, t_i^4, \cdots$ denote the discrete instances when the ith subsystem is reactivated; $t_i^1, t_i^3, \cdots$ denote the discrete instances when the ith subsystem is inactivated and another subsystem is activated.

For $\forall i \in \mathbf{\Omega}$

$$\begin{aligned} \dot{V}_i(t) = {} & \dot{\boldsymbol{e}}^{\mathrm{T}}(t)\mathbf{P}\boldsymbol{e}(t) + \boldsymbol{e}^{\mathrm{T}}(t)\mathbf{P}\dot{\boldsymbol{e}}(t) \\ & + 2\left(\mathbf{B}^{\mathrm{T}}\mathbf{P}\boldsymbol{e}(t)\right)^{\mathrm{T}} \left[\int_0^t \mathbf{K}\mathbf{B}^{\mathrm{T}}\mathbf{P}\boldsymbol{e}(\tau)\boldsymbol{x}^{\mathrm{T}}(\tau)\,\mathrm{d}\tau\right]\boldsymbol{x}(t) \\ & + 2\left(\mathbf{B}^{\mathrm{T}}\mathbf{P}\boldsymbol{e}(t)\right)^{\mathrm{T}} \boldsymbol{\alpha}_i \mathbf{B}^{\mathrm{T}}\mathbf{P}\boldsymbol{e}(t)\boldsymbol{x}^{\mathrm{T}}(t)\boldsymbol{x}(t) \\ & + 2\left(\mathbf{B}^{\mathrm{T}}\mathbf{P}\boldsymbol{e}(t)\right)^{\mathrm{T}} \left[\int_0^t \mathbf{L}\mathbf{B}^{\mathrm{T}}\mathbf{P}\boldsymbol{e}(\tau)\boldsymbol{r}^{\mathrm{T}}(\tau)\,\mathrm{d}\tau\right]\boldsymbol{r}(t) \\ & + 2\left(\mathbf{B}^{\mathrm{T}}\mathbf{P}\boldsymbol{e}(t)\right)^{\mathrm{T}} \boldsymbol{\beta}_i \mathbf{B}^{\mathrm{T}}\mathbf{P}\boldsymbol{e}(t)\boldsymbol{r}^{\mathrm{T}}(t)\boldsymbol{r}(t) \end{aligned} \tag{11}$$

Substitute equation (8) into equation (11) and then by equation (9), the following equation (12) holds, i.e. each subsystem is globally asymptotically stable

$$\begin{aligned} \dot{V}_i = {} & \boldsymbol{e}^{\mathrm{T}}(t)\left(\mathbf{A}_{\mathrm{m_i}}^{\mathrm{T}}\mathbf{P} + \mathbf{P}\mathbf{A}_{\mathrm{m_i}}\right)\boldsymbol{e}(t) - 2\boldsymbol{e}^{\mathrm{T}}(t)\mathbf{P}\mathbf{B}\boldsymbol{d}(t) \\ & - 2\delta(t)\boldsymbol{e}^{\mathrm{T}}(t)\mathbf{P}\mathbf{B}\,\mathrm{sgn}\left(\mathbf{B}^{\mathrm{T}}\mathbf{P}\boldsymbol{e}(t)\right) \\ < {} & -\boldsymbol{e}^{\mathrm{T}}(t)\mathbf{Z}\boldsymbol{e}(t) - 2\boldsymbol{e}^{\mathrm{T}}(t)\mathbf{P}\mathbf{B}\boldsymbol{d}(t) \\ & - 2\delta(t)\boldsymbol{e}^{\mathrm{T}}(t)\mathbf{P}\mathbf{B}\,\mathrm{sgn}\left(\mathbf{B}^{\mathrm{T}}\mathbf{P}\boldsymbol{e}(t)\right) \\ < {} & -\rho_{\min}(\mathbf{Z})\|\boldsymbol{e}(t)\|^2 + 2\delta(t)\left\|\mathbf{B}^{\mathrm{T}}\mathbf{P}\boldsymbol{e}(t)\right\| - 2\delta(t)\left\|\mathbf{B}^{\mathrm{T}}\mathbf{P}\boldsymbol{e}(t)\right\|_1 \\ < {} & -\rho_{\min}(\mathbf{Z})\|\boldsymbol{e}(t)\|^2 + 2\delta(t)\left\|\mathbf{B}^{\mathrm{T}}\mathbf{P}\boldsymbol{e}(t)\right\| - 2\delta(t)\left\|\mathbf{B}^{\mathrm{T}}\mathbf{P}\boldsymbol{e}(t)\right\| \\ < {} & 0 \end{aligned} \tag{12}$$

Step 2: In what follows the globally asymptotical stability of the closed-loop switched system is proved.

Denote

$$\begin{aligned} & \int_0^t \Gamma(\boldsymbol{e}, \boldsymbol{x}, \boldsymbol{r})\,\mathrm{d}t' \\ & = 2\int_0^t \left(\mathbf{B}^{\mathrm{T}}\mathbf{P}\boldsymbol{e}(t')\right)^{\mathrm{T}} \left(\int_0^{t'} \mathbf{K}\mathbf{B}^{\mathrm{T}}\mathbf{P}\boldsymbol{e}(\tau)\boldsymbol{x}^{\mathrm{T}}(\tau)\,\mathrm{d}\tau\right)\boldsymbol{x}(t')\,\mathrm{d}t' \\ & \quad + 2\int_0^t \left(\mathbf{B}^{\mathrm{T}}\mathbf{P}\boldsymbol{e}(t')\right)^{\mathrm{T}} \left(\int_0^{t} \mathbf{L}\mathbf{B}^{\mathrm{T}}\mathbf{P}\boldsymbol{e}(\tau)\boldsymbol{r}^{\mathrm{T}}(\tau)\,\mathrm{d}\tau\right)\boldsymbol{r}(t')\,\mathrm{d}t' \end{aligned} \tag{13}$$

$$\begin{aligned} & \int_{\Im(t_i^0,\, t_i^s,\, t)} \Phi(\boldsymbol{e}, \boldsymbol{x}, \boldsymbol{r})\,\mathrm{d}t' \\ & = 2\int_{\Im(t_i^0,\, t_i^s,\, t)} \left(\mathbf{B}^{\mathrm{T}}\mathbf{P}\boldsymbol{e}(t')\right)^{\mathrm{T}} \boldsymbol{\alpha}_i \mathbf{B}^{\mathrm{T}}\mathbf{P}\boldsymbol{e}(t')\boldsymbol{x}^{\mathrm{T}}(t')\boldsymbol{x}(t')\,\mathrm{d}t' \\ & \quad + 2\int_{\Im(t_i^0,\, t_i^s,\, t)} \left(\mathbf{B}^{\mathrm{T}}\mathbf{P}\boldsymbol{e}(t')\right)^{\mathrm{T}} \boldsymbol{\beta}_i \mathbf{B}^{\mathrm{T}}\mathbf{P}\boldsymbol{e}(t')\boldsymbol{r}^{\mathrm{T}}(t')\boldsymbol{r}(t')\,\mathrm{d}t' \end{aligned} \tag{14}$$

Then, equation (10) can be rewritten as

$$V_i = \boldsymbol{e}^{\mathrm{T}}(t)\mathbf{P}\boldsymbol{e}(t) + \int_0^t \Gamma(\boldsymbol{e}, \boldsymbol{x}, \boldsymbol{r})\,\mathrm{d}t' + \int_{\Im(t_i^0,\, t_i^s,\, t)} \Phi(\boldsymbol{e}, \boldsymbol{x}, \boldsymbol{r})\,\mathrm{d}t' \tag{15}$$

and it is easy to verify that

$$\int_{\Im(t_i^0,\, t_i^s,\, t)} \Phi(\boldsymbol{e}, \boldsymbol{x}, \boldsymbol{r})\,\mathrm{d}t' > 0$$

$$\text{and } \frac{\mathrm{d}}{\mathrm{d}t}\left(\int_{\Im(t_i^0,\, t_i^s,\, t)} \Phi(\boldsymbol{e}, \boldsymbol{x}, \boldsymbol{r})\,\mathrm{d}t'\right) > 0$$

Let t_m^p and t_m^q denote the times at which the mth subsystem is consecutively activated. Without loss of generality, suppose that the condition $q=p+2$ holds, i.e. an unknown nth subsystem is activated at the time $t_n^r \in (t_m^p, t_m^q)$ and remains active during the time interval $[t_n^r, t_m^{q-}]$.

Considering $t \in [t_n^r, t_m^{q-}]$, $\dot{V}_n < 0$, hence

$$\begin{aligned} & V_n(t_n^r) > V_n(t_m^{q-}) \\ & \Rightarrow \boldsymbol{e}^{\mathrm{T}}(t_n^r)\mathbf{P}\boldsymbol{e}(t_n^r) + \int_0^{t_n^r} \Gamma(\boldsymbol{e}, \boldsymbol{x}, \boldsymbol{r})\,\mathrm{d}t' \\ & \quad + \int_{\Im(t_n^0, t_n^r, t_n^r)} \Phi(\boldsymbol{e}, \boldsymbol{x}, \boldsymbol{r})\,\mathrm{d}t' > \boldsymbol{e}^{\mathrm{T}}(t_m^{q-})\mathbf{P}\boldsymbol{e}(t_m^{q-}) \\ & \quad + \int_0^{t_m^{q-}} \Gamma(\boldsymbol{e}, \boldsymbol{x}, \boldsymbol{r})\,\mathrm{d}t' + \int_{\Im(t_n^0, t_n^r, t_m^{q-})} \Phi(\boldsymbol{e}, \boldsymbol{x}, \boldsymbol{r})\,\mathrm{d}t' \\ & \Rightarrow \boldsymbol{e}^{\mathrm{T}}(t_n^r)\mathbf{P}\boldsymbol{e}(t_n^r) + \int_0^{t_n^r} \Gamma(\boldsymbol{e}, \boldsymbol{x}, \boldsymbol{r})\,\mathrm{d}t' > \boldsymbol{e}^{\mathrm{T}}(t_m^{q-})\mathbf{P}\boldsymbol{e}(t_m^{q-}) \\ & \qquad + \int_0^{t_m^{q-}} \Gamma(\boldsymbol{e}, \boldsymbol{x}, \boldsymbol{r})\,\mathrm{d}t' \end{aligned} \tag{16}$$

Because $\boldsymbol{x}(t)$ and $\boldsymbol{x}_{\mathrm{m}}(t)$ are continuous at each switching, the error $\boldsymbol{e}(t)=\boldsymbol{x}_{\mathrm{m}}(t)-\boldsymbol{x}(t)$ is continuous such that

$$\begin{aligned} & \boldsymbol{e}^{\mathrm{T}}(t_n^r)\mathbf{P}\boldsymbol{e}(t_n^r) + \int_0^{t_n^r} \Gamma(\boldsymbol{e}, \boldsymbol{x}, \boldsymbol{r})\,\mathrm{d}t' > \boldsymbol{e}^{\mathrm{T}}(t_m^{q-})\mathbf{P}\boldsymbol{e}(t_m^{q-}) \\ & \qquad + \int_0^{t_m^{q-}} \Gamma(\boldsymbol{e}, \boldsymbol{x}, \boldsymbol{r})\,\mathrm{d}t' \\ & \Rightarrow \boldsymbol{e}^{\mathrm{T}}(t_n^{r-})\mathbf{P}\boldsymbol{e}(t_n^{r-}) + \int_0^{t_n^{r-}} \Gamma(\boldsymbol{e}, \boldsymbol{x}, \boldsymbol{r})\,\mathrm{d}t' > \boldsymbol{e}^{\mathrm{T}}(t_m^q)\mathbf{P}\boldsymbol{e}(t_m^q) \\ & \qquad + \int_0^{t_m^q} \Gamma(\boldsymbol{e}, \boldsymbol{x}, \boldsymbol{r})\,\mathrm{d}t' \end{aligned} \tag{17}$$

Furthermore, since $\Im(t_m^0, t_m^q, t_m^q) = \Im(t_m^0, t_m^p, t_n^{r-}) \cup \{t_m^q\}$, it holds that

$$\int_{\Im(t_m^0, t_m^p, t_n^{r-})} \Phi(\boldsymbol{e}, \boldsymbol{x}, \boldsymbol{r})\,\mathrm{d}t' = \int_{\Im(t_m^0, t_m^q, t_m^q)} \Phi(\boldsymbol{e}, \boldsymbol{x}, \boldsymbol{r})\,\mathrm{d}t'$$

Therefore, by equation (17), it can be obtained that

$$\begin{aligned} & \boldsymbol{e}^{\mathrm{T}}(t_n^{r-})\mathbf{P}\boldsymbol{e}(t_n^{r-}) + \int_0^{t_n^{r-}} \Gamma(\boldsymbol{e}, \boldsymbol{x}, \boldsymbol{r})\,\mathrm{d}t' \\ & \quad + \int_{\Im(t_m^0, t_m^p, t_n^{r-})} \Phi(\boldsymbol{e}, \boldsymbol{x}, \boldsymbol{r})\,\mathrm{d}t' > \boldsymbol{e}^{\mathrm{T}}(t_m^q)\mathbf{P}\boldsymbol{e}(t_m^q) \\ & \quad + \int_0^{t_m^q} \Gamma(\boldsymbol{e}, \boldsymbol{x}, \boldsymbol{r})\,\mathrm{d}t' + \int_{\Im(t_m^0, t_m^q, t_m^q)} \Phi(\boldsymbol{e}, \boldsymbol{x}, \boldsymbol{r})\,\mathrm{d}t' \\ & \Rightarrow V_m(t_n^{r-}) > V_m(t_m^q) \end{aligned} \tag{18}$$

This means that when the mth subsystem is reactivated at t_m^q, the value of the Lyapunov function is monotonically decreasing when compared with that at t_n^{r-} when the mth subsystem is inactivated last time, which is also depicted in Fig. 4. By Lemma 2, it can be concluded that the closed-loop switched system is globally asymptotically stable.

Considering the inequality (9), the autonomous switched reference system $\dot{\boldsymbol{x}}_{\mathrm{m}}(t) = \mathbf{A}_{\mathrm{m}_\sigma}\boldsymbol{x}_{\mathrm{m}}(t)$ shares a common Lyapunov function $\tilde{V} = \boldsymbol{x}_{\mathrm{m}}^{\mathrm{T}}(t)\mathbf{P}\boldsymbol{x}_{\mathrm{m}}(t)$, therefore the system (2) is input-to-state stable [**9**], i.e. $\boldsymbol{x}_{\mathrm{m}}(t)$ must be bounded for any bounded input $\boldsymbol{r}(t)$. Therefore, the state $\boldsymbol{x}(t) = \boldsymbol{x}_{\mathrm{m}}(t) - \boldsymbol{e}(t)$ of the system (1) must be bounded under arbitrary switchings.

Remark 4

If $\boldsymbol{\alpha}_i$, $\boldsymbol{\beta}_i$ are set to be positive constant matrices $\boldsymbol{\alpha}$, $\boldsymbol{\beta}$, just as $\mathbf{K}$ and $\mathbf{L}$, a common Lyapunov function can be achieved for the closed-loop switched system (this result is easy to obtain from equation (10)), hence the globally asymptotical stability is directly ensured [**9**]. Additionally, the proportion parts of the feedback and feedforward controllers do not need to be zero when the corresponding subsystem and the controller are 'switched off', whereas they can be continuously adjusted. The price to be paid for such a scheme is that the desired performance may be hard to achieve, because all the adaptive gains are constant, i.e. the controller gains corresponding to S1 are the same as the gains corresponding to all subcontrollers of S2. In order to alleviate this problem, the MRASC scheme presented in this study achieves the better performance trade-off by allowing $\boldsymbol{\alpha}_i$, $\boldsymbol{\beta}_i$ to be set arbitrarily, and the proportion parts in the feedforward and feedback controllers are set to be zero when the controller is 'switched off'.

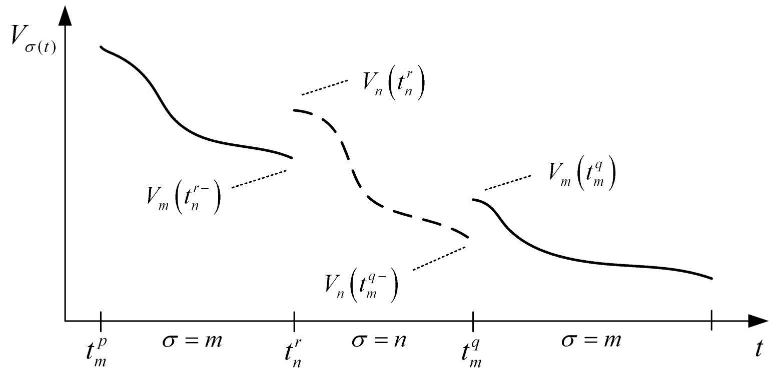

Fig. 4 A generic evolution of the Lyapunov function associated with the closed-loop switched system

Remark 5

The loss of effectiveness failure of actuator probably makes the actuator saturate. For this situation, the MRASC scheme is also valid. Stability of the closed-loop switched system and a desired performance can be ensured, provided that the adaptive gains $\mathbf{K}$, $\mathbf{L}$, $\boldsymbol{\alpha}_i$, $\boldsymbol{\beta}_i$ are all diagonal matrices and reset to be $\mathbf{K}'$, $\mathbf{L}'$, $\boldsymbol{\alpha}_i'$, $\boldsymbol{\beta}_i'$ according to the degree of loss effectiveness when the actuator fault occurs. Suppose that $\boldsymbol{\Lambda} = \mathrm{diag}(\lambda_1, \lambda_2, \lambda_3)$, $\lambda_j \in (0, 1)$, $j = 1, 2, 3$ specifies the degree of loss of effectiveness for the inputs, the non-smooth non-linear term $\delta(t)\,\mathrm{sgn}\left(\mathbf{B}^{\mathrm{T}}\mathbf{P}\boldsymbol{e}(t)\right)$ should be changed to $\delta(t)\,\mathrm{sgn}\left((\mathbf{B}\boldsymbol{\Lambda})^{\mathrm{T}}\mathbf{P}\boldsymbol{e}(t)\right)$ and $\mathbf{K}$, $\mathbf{L}$, $\boldsymbol{\alpha}_i$, $\boldsymbol{\beta}_i$, $\mathbf{F}_i\left(t_i^0\right)$, $\mathbf{G}_i\left(t_i^0\right)$ should be reset to be $\mathbf{K}'$, $\mathbf{L}'$, $\boldsymbol{\alpha}_i'$, $\boldsymbol{\beta}_i'$, $\mathbf{F}_i'\left(t_i^0\right)$, $\mathbf{G}_i'\left(t_i^0\right)$, respectively,

$$\begin{aligned}
&\mathbf{K}' = \mathbf{K}\left(\boldsymbol{\Lambda}^{-1}\right)^2, \ \mathbf{L}' = \mathbf{L}\left(\boldsymbol{\Lambda}^{-1}\right)^2, \ \boldsymbol{\alpha}'_i = \boldsymbol{\alpha}_i\left(\boldsymbol{\Lambda}^{-1}\right)^2, \\
&\boldsymbol{\beta}_i' = \boldsymbol{\beta}_i\left(\boldsymbol{\Lambda}^{-1}\right)^2 \\
&\mathbf{A}_{\mathrm{m_i}} - \mathbf{A} = \mathbf{B}\boldsymbol{\Lambda}\mathbf{F}_i'\left(t_i^0\right), \ \mathbf{B}_{\mathrm{m_i}} - \mathbf{B}\boldsymbol{\Lambda} = \mathbf{B}\boldsymbol{\Lambda}\mathbf{G}_i'\left(t_i^0\right)
\end{aligned} \tag{19}$$

such that

$$\begin{aligned}
&\int_0^t \left((\mathbf{B}\boldsymbol{\Lambda})^{\mathrm{T}}\mathbf{P}\boldsymbol{e}(t')\right)^{\mathrm{T}} \left(\int_0^{t'} \mathbf{K}'(\mathbf{B}\boldsymbol{\Lambda})^{\mathrm{T}}\mathbf{P}\boldsymbol{e}(\tau)\boldsymbol{x}^{\mathrm{T}}(\tau)\,\mathrm{d}\tau\right)\boldsymbol{x}(t')\,\mathrm{d}t' \\
&\quad = \int_0^t \left(\mathbf{B}^{\mathrm{T}}\mathbf{P}\boldsymbol{e}(t')\right)^{\mathrm{T}} \left(\int_0^{t'} \mathbf{K}\mathbf{B}^{\mathrm{T}}\mathbf{P}\boldsymbol{e}(\tau)\boldsymbol{x}^{\mathrm{T}}(\tau)\,\mathrm{d}\tau\right)\boldsymbol{x}(t')\,\mathrm{d}t' \\
&\int_{\Im(t_i^0, t_i^s, t)} \left((\mathbf{B}\boldsymbol{\Lambda})^{\mathrm{T}}\mathbf{P}\boldsymbol{e}(t')\right)^{\mathrm{T}} \boldsymbol{\alpha}'_i(\mathbf{B}\boldsymbol{\Lambda})^{\mathrm{T}}\mathbf{P}\boldsymbol{e}(t')\boldsymbol{x}^{\mathrm{T}}(t')\boldsymbol{x}(t')\,\mathrm{d}t' \\
&\quad = \int_{\Im(t_i^0, t_i^s, t)} \left(\mathbf{B}^{\mathrm{T}}\mathbf{P}\boldsymbol{e}(t')\right)^{\mathrm{T}} \boldsymbol{\alpha}_i\mathbf{B}^{\mathrm{T}}\mathbf{P}\boldsymbol{e}(t')\boldsymbol{x}^{\mathrm{T}}(t')\boldsymbol{x}(t')\,\mathrm{d}t'
\end{aligned} \tag{20}$$

and similar integral equations also hold for the gains $\mathbf{L}'$, $\mathbf{L}$ and $\boldsymbol{\beta}_i'$, $\boldsymbol{\beta}_i$.

Thus, the candidate Lyapunov function in equation (10) is still valid for the subsystems of the closed-loop switched system when faults occur. The rest of the proof for stability is similar to that of Theorem 1 and hence is omitted here. The anti-saturation performance of the MRASC scheme with the occurrence of actuator fault will be validated by the simulation in section 4.

4 SIMULATION

4.1 Simulation Description

To validate the MRASC scheme derived in the previous sections, simulations have been performed using the AHFV model presented in section 1.

Suppose that the loss of effectiveness failure of the actuator takes place at a certain time, which is likely to induce an actuator saturation event. When this fault occurs, a switching action arises and an appropriate subsystem of the SRS and corresponding controller of the SAC are selected to control the AHFV. Note that it is assumed that the fault detection and diagnosis mechanisms are perfect and thus the actuator fault and switching action arise simultaneously.

The plant of the AHFV is described by

$$\begin{aligned}
&\dot{\boldsymbol{x}}(t) = \mathbf{A}\boldsymbol{x}(t) + \mathbf{B}\boldsymbol{\Lambda}(\boldsymbol{u}(t) + \boldsymbol{d}(t)), \quad \boldsymbol{\Lambda} = \mathrm{diag}(\lambda_1, \lambda_2, \lambda_3) \\
&\boldsymbol{x}(0) = (0, 0, 0, 0, 0, 0, 0)^{\mathrm{T}}
\end{aligned} \tag{21}$$

where $\boldsymbol{\Lambda}$ is utilized to describe the loss effectiveness failure of the actuator and λ_i is an unknown parameter that specifies the degree of loss effectiveness

$$\begin{cases} 0<\lambda_i<1, \\ \text{if the } i\text{th control input fails, } i=1,\,2,\,3 \\ \lambda_i=1, \\ \text{if the } i\text{th control input does not fail, } i=1,\,2,\,3 \end{cases}$$

The disturbance $\mathbf{D}(t)=\mathbf{B}\boldsymbol{\Lambda}\boldsymbol{d}(t)$ is composed of atmospheric disturbance $\boldsymbol{d}_1(t)$ and pitch rate measure disturbance $\boldsymbol{d}_2(t)$

$$\mathbf{D}(t)=\boldsymbol{d}_1(t)+\boldsymbol{d}_2(t)$$

$$\boldsymbol{d}_1(t)=\mathbf{B}_\mathrm{g}V_\mathrm{g}(t), \qquad \mathbf{B}_\mathrm{g}=(0, a_{22}, a_{32}, 0, a_{52}, 0, 0)^\mathrm{T}$$

$$\boldsymbol{d}_2(t)=(0, 0, 0, 0, 0.0087, 0, 0)^\mathrm{T}$$

where the elements in $\mathbf{B}_\mathrm{g}$ are the corresponding elements of the matrix $\mathbf{A}$, $V_\mathrm{g}(t)$ is generated by passing white noise through transfer function $F_u(s)=\sqrt{2V_0\sigma_u^2/L_u}\Big/(s+V_0/L_u)$, and $V_0=8976\,\mathrm{ft/s}$, $\sigma_u=6.006\,\mathrm{ft/s}$, $L_u=3135\,\mathrm{ft}$ [**16**, **17**].

Supposing $\boldsymbol{\Lambda}=\boldsymbol{T}$, the upper bound $\delta(t)$ for $\boldsymbol{d}(t)$ can be selected as $\|\mathbf{B}\|^{-1}\|\mathbf{D}(t)\|=2\times10^{-5}$, where $\|\mathbf{D}(t)\|=0.0133$. Note that the value for the disturbance $\boldsymbol{d}_1(t)$ is evaluated by a simple simulation programmed by MATLAB R2007 in advance, where the sample time for the Gaussian Noise Generator Block is 0.02.

The switched reference system is given as

$$\dot{\boldsymbol{x}}_\mathrm{m}(t)=\mathbf{A}_{\mathrm{m}_\sigma}\boldsymbol{x}_\mathrm{m}(t)+\mathbf{B}_{\mathrm{m}_\sigma}\boldsymbol{r}(t), \quad \sigma(t,\psi)\to\{1,2\} \qquad (22)$$

where ψ denotes the occurrence of the fault, i.e. $\sigma(t,\psi)=2$ when the fault takes place, otherwise, $\sigma(t,\psi)=1$

$$\mathbf{A}_{\mathrm{m}_1}=\mathbf{A}_{\mathrm{m}_2}=\begin{bmatrix} 0 & 0 & -7924.8 & 7924.8 & 0 & 0 & 0 \\ 0.004\,3991 & -0.001\,0132 & -729.43 & 716.69 & -6.6258 & 1.5351 & 0.487\,48 \\ -0.000\,363\,03 & 1.3927\times10^{-5} & 38.067 & -36.969 & 1.6104 & -0.132\,41 & -0.041\,481 \\ 0 & 0 & 0 & 0 & 1 & 0 & 0 \\ 0.018\,978 & -0.000\,399\,66 & -2344.3 & 2287.5 & -37.441 & 6.8457 & 2.5425 \\ 0 & 0 & 0 & 0 & 0 & 0 & 1 \\ -0.099\,724 & 0.009\,1715 & 115\,64 & -112\,66 & 100.05 & -35.939 & -8.612 \end{bmatrix}$$

$$\mathbf{B}_{\mathrm{m}_1}=\mathbf{B},\ \mathbf{B}_{\mathrm{m}_2}=\mathbf{B}\boldsymbol{\Lambda}$$

with the desired eigenvalues $\{-2.39\pm16.9\mathrm{j}\ \ -1.6\pm2.5\mathrm{j}\ \ -0.001\pm0.001\mathrm{j}\ \ -0.005\}$.

The reference input

$$\boldsymbol{r}(t) = -\bar{\mathbf{R}}^{-1}\mathbf{B}_{\mathrm{m}_1}^\mathrm{T}\left[\bar{\mathbf{K}}\boldsymbol{x}_\mathrm{m}(t)-\left[\bar{\mathbf{K}}\mathbf{B}_{\mathrm{m}_1}\bar{\mathbf{R}}^{-1}\mathbf{B}_{\mathrm{m}_1}^\mathrm{T}-\mathbf{A}_{\mathrm{m}_1}^\mathrm{T}\right]^{-1}\bar{\mathbf{Q}}\boldsymbol{c}(t)\right],$$

$$\bar{\mathbf{Q}},\ \bar{\mathbf{R}}>0$$

where

$$\bar{\mathbf{Q}}=[1/400, 1/100, 1/0.017, 1/0.017, 1/0.017, 10, 10]^\mathrm{T}, \quad \bar{\mathbf{R}}=[1/0.017, 1, 1]^\mathrm{T}$$

$$\bar{\mathbf{K}}=\begin{bmatrix} 0.015\,441 & 0.0018 & -28.218 & 25.721 & -0.520\,91 & 0.192\,42 & -0.002\,1212 \\ 0.0018 & 0.001\,7886 & -18.19 & 17.076 & -0.345\,71 & 0.101\,83 & -0.001\,9396 \\ -28.218 & -18.19 & 3.7173\times10^5 & -3.5512\times10^5 & 6006 & -1496.3 & 18.671 \\ 25.721 & 17.076 & -3.5512\times10^5 & 3.397\times10^5 & -5690.2 & 1394.4 & -17.233 \\ -0.520\,91 & -0.345\,71 & 6006 & -5690.2 & 106.34 & -28.528 & 0.417\,86 \\ 0.192\,42 & 0.101\,83 & -1496.3 & 1394.4 & -28.528 & 19.757 & -0.098\,345 \\ -0.002\,1212 & -0.001\,9396 & 18.671 & -17.233 & 0.417\,86 & -0.098\,345 & 0.034\,383 \end{bmatrix}$$

The altitude and flight velocity commands are illustrated in Fig. 5 and the other commands are all set to be zero.

The adaptive gains of the SAC are given as follows

$$\mathbf{K}_1 = \mathbf{L}_1 = \boldsymbol{\alpha}_1 = \boldsymbol{\beta}_1 = \mathrm{diag}(0.01, 0.01, 0.01)$$

$$\mathbf{K}_2 = \mathbf{L}_2 = \boldsymbol{\alpha}_2 = \boldsymbol{\beta}_2 = \mathrm{diag}(0.01, 0.01, 0.01)\left(\boldsymbol{\Lambda}^{-1}\right)^2$$

Set $\mathbf{Z} = \mathrm{diag}\left(10^{-17}/4, 10^{-17}, 10^{-13}/1.7, 10^{-13}/1.7, 10^{-13}/1.7, 10^{-16}, 10^{-16}\right)$, then there exists a $\mathbf{P} > 0$ that satisfies the inequality (9) such that Theorem 1 holds. Namely, the closed-loop switched system corresponding to the MRASC scheme is globally asymptotically stable under the arbitrary switching law

$$\mathbf{P} = \begin{bmatrix} 1.0383\times10^{-14} & -2.3121\times10^{-13} & 3.2920\times10^{-12} & -1.0307\times10^{-11} & -3.0904\times10^{-13} & 3.3900\times10^{-13} & -8.0872\times10^{-14} \\ -2.3121\times10^{-13} & 1.5416\times10^{-11} & -4.2377\times10^{-10} & 5.7781\times10^{-10} & 8.3007\times10^{-13} & -6.7354\times10^{-12} & 2.3773\times10^{-12} \\ 3.2920\times10^{-12} & -4.2377\times10^{-10} & 0 & 0 & 2.6650\times10^{-10} & 1.7284\times10^{-10} & -8.7432\times10^{-11} \\ -1.0307\times10^{-11} & 5.7781\times10^{-10} & 0 & 0 & 4.6618\times10^{-11} & -5.2087\times10^{-10} & 1.7119\times10^{-10} \\ -3.0904\times10^{-13} & 8.3007\times10^{-13} & 2.6650\times10^{-10} & 4.6618\times10^{-11} & 2.0865\times10^{-11} & -1.5938\times10^{-11} & 3.1050\times10^{-12} \\ 3.3900\times10^{-13} & -6.7354\times10^{-12} & 1.7284\times10^{-10} & -5.2087\times10^{-10} & -1.5938\times10^{-11} & 1.7004\times10^{-11} & -3.9589\times10^{-12} \\ -8.0872\times10^{-14} & 2.3773\times10^{-12} & -8.7432\times10^{-11} & 1.7119\times10^{-10} & 3.1050\times10^{-12} & -3.9589\times10^{-12} & 1.0185\times10^{-12} \end{bmatrix}$$

4.2 Evaluation

Suppose that the actuator fault happens at 220 s.

In the following, two cases, which describe different degrees of the loss of effectiveness of the actuator, will be simulated to investigate the anti-saturation performance of the MRASC scheme. The classical MRAC scheme (i.e. the adaptive controller is without the switching actions and the non-smooth non-linear term) is also adopted for each case, in order to compare the performance with the proposed MRASC scheme.

Case 1

In this case $\boldsymbol{\Lambda} = \mathrm{diag}(0.9, 1, 1)$, i.e. the pitch control surface fails. The results are depicted in Figs 6 to 15.

From these figures it can be concluded that the MRASC scheme achieves a satisfactory performance. State trajectories controlled by the MRASC scheme are much smoother than those controlled by the MRAC scheme. It is more attractive that the control inputs, including the pitch control surface deflection, the diffuser area ratio, and the fuel mass flowrate, are much smoother as compared to those obtained when the system is controlled by the MRAC scheme, which is depicted in Figs 13 to 15. In particular, the value of the diffuser area ratio under the MRAC scheme exceeds the upper bound of 0.85, whereas the value of the diffuser area ratio under the MRASC scheme is much smaller and smoother.

Case 2

In this case $\boldsymbol{\Lambda} = \mathrm{diag}(1, 0.75, 1)$, i.e. the diffuser area ratio fails. This case is more severe than Case 1, because under the MRAC scheme all the states and

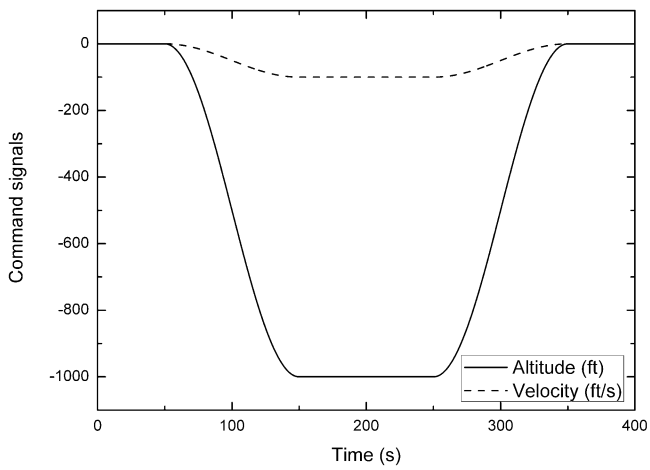

Fig. 5 Altitude command and flight velocity command

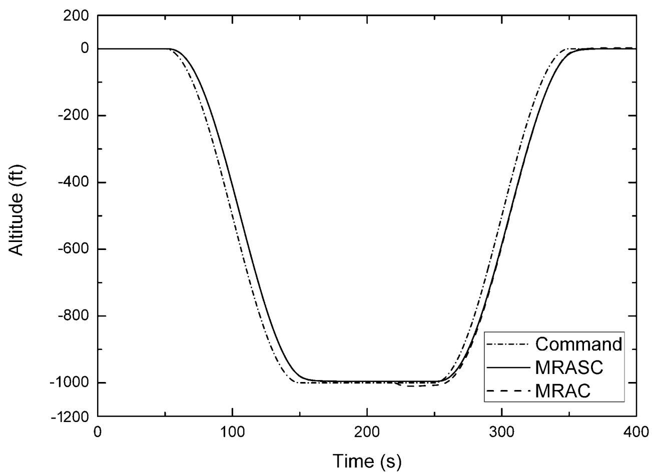

Fig. 6 Trajectories of the altitude for Case 1

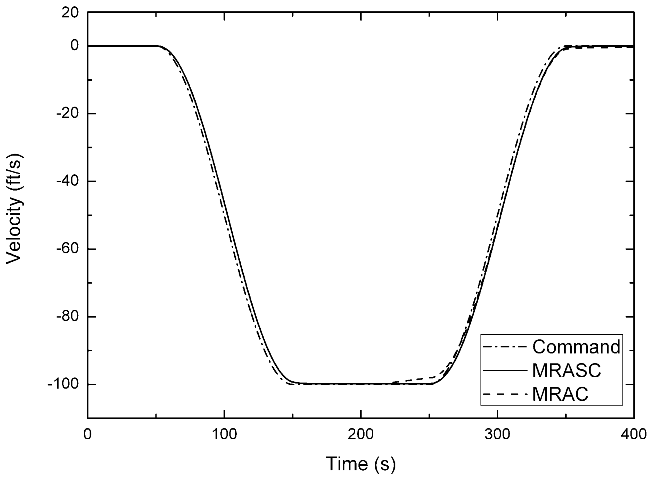

Fig. 7 Trajectories of the flight velocity for Case 1

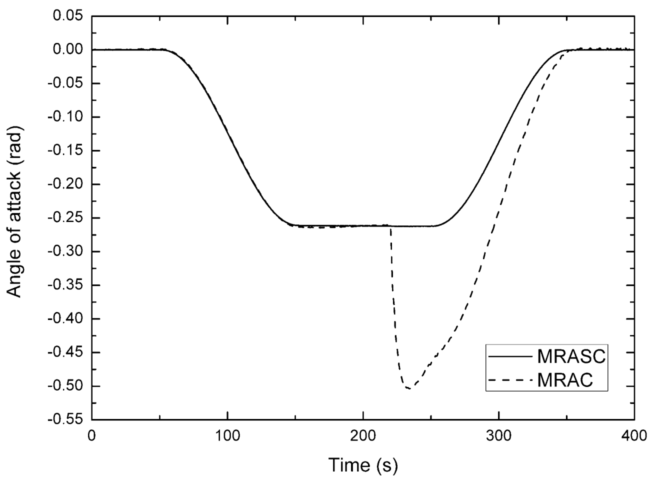

Fig. 8 Trajectories of the angle of attack for Case 1

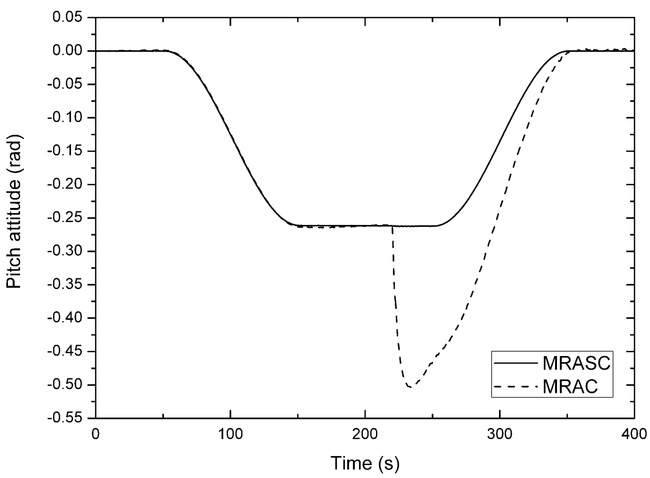

Fig. 9 Trajectories of the pitch attitude for Case 1

control inputs diverge quickly and the system is unstable after the fault occurs. The trajectories of the altitude and the diffuser area ratio are depicted in

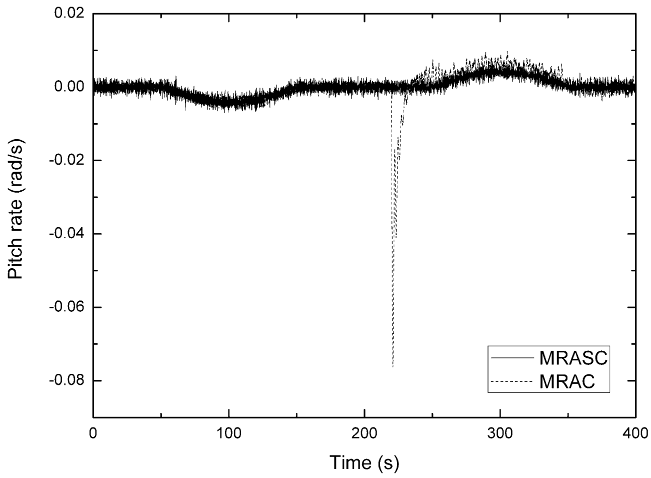

Fig. 10 Trajectories of the pitch rate for Case 1

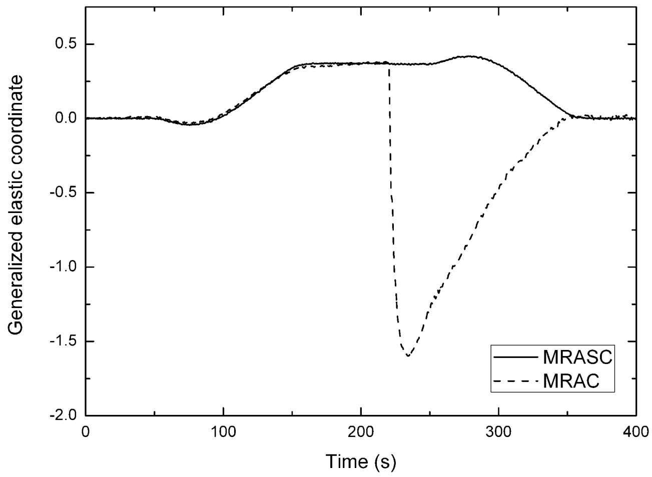

Fig. 11 Trajectories of the generalized elastic coordinate for Case 1

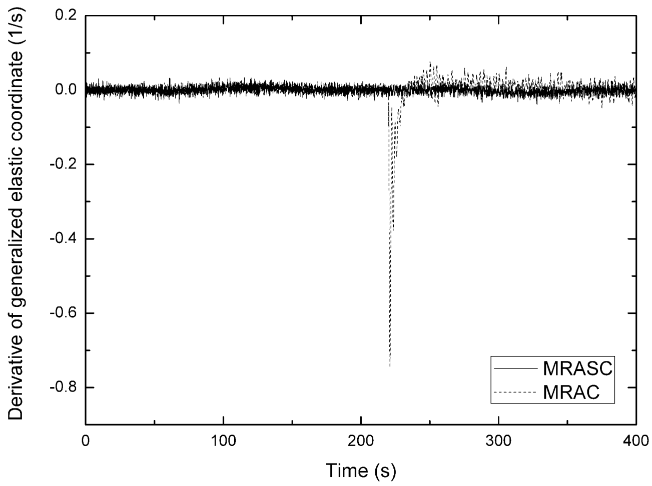

Fig. 12 Trajectories of the derivate of the generalized elastic coordinate for Case 1

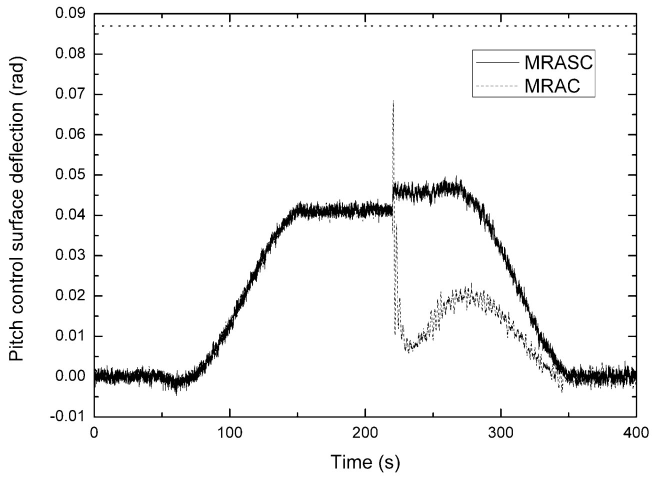

Fig. 13 Trajectories of the pitch control surface deflection for Case 1

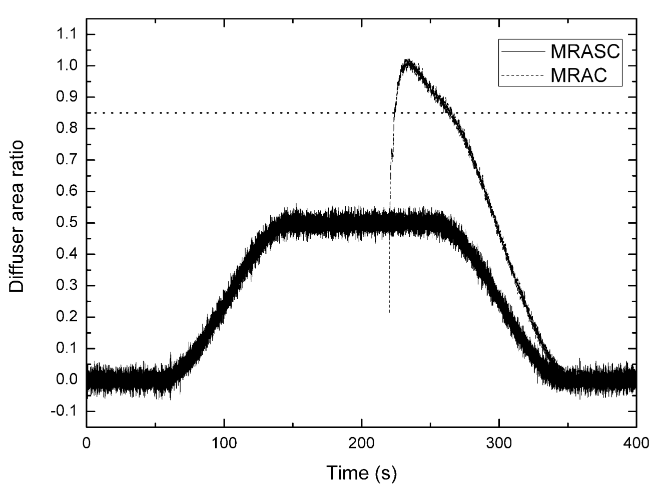

Fig. 14 Trajectories of the diffuser area ratio for Case 1

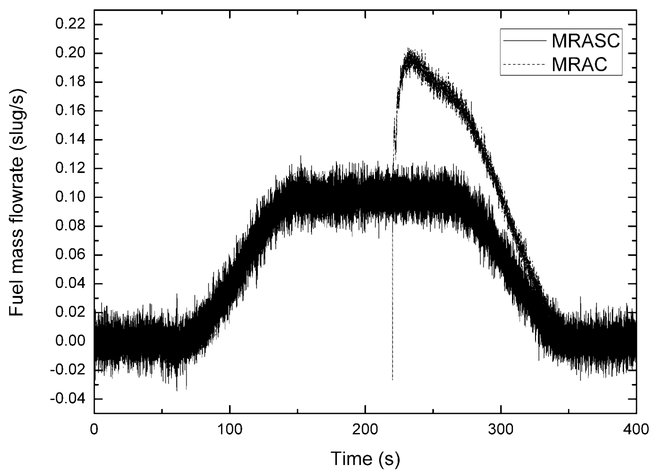

Fig. 15 Trajectories of the fuel mass flowrate for Case 1

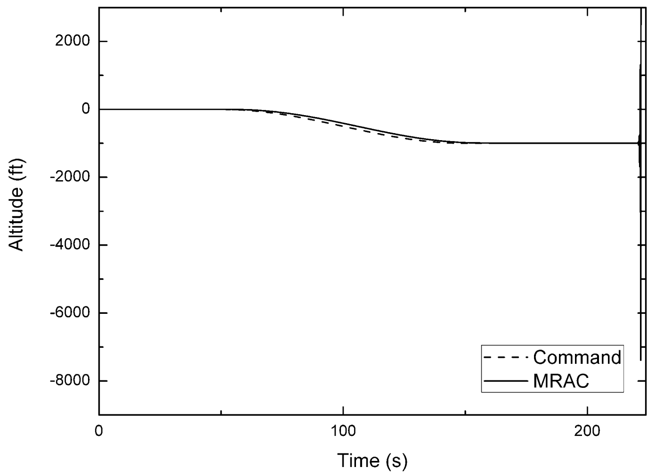

Fig. 16 Trajectory of the altitude under the MRAC scheme for Case 2

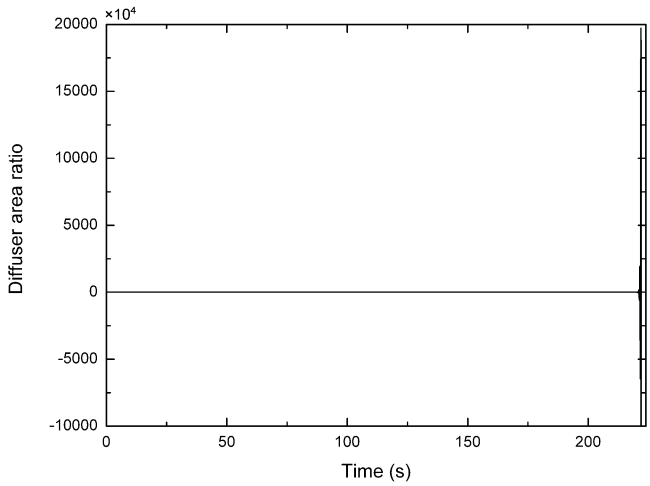

Fig. 17 Trajectory of the diffuser area ratio under the MRAC scheme for Case 2

Figs 16 and 17 to show the phenomenon of the instability. Even though, the same conclusion can be achieved. The proposed MRASC scheme obtains a satisfactory performance with smoother control inputs, and all the inputs satisfy the constraints, which is depicted in Figs 18 to 27.

In conclusion, simulation results demonstrate the effectiveness of the MRASC scheme for controlling the AHFV with actuator saturation. Additionally, the proposed scheme performs much better than the classical MRAC adaptive control scheme.

5 CONCLUSIONS

An MRASC scheme for the control of AHFVs with actuator saturation is proposed. In contrast to most

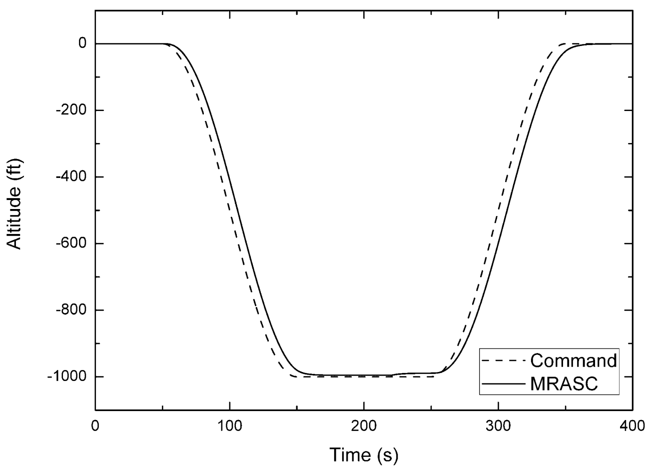

Fig. 18 Trajectory of the altitude under the MRASC scheme for Case 2

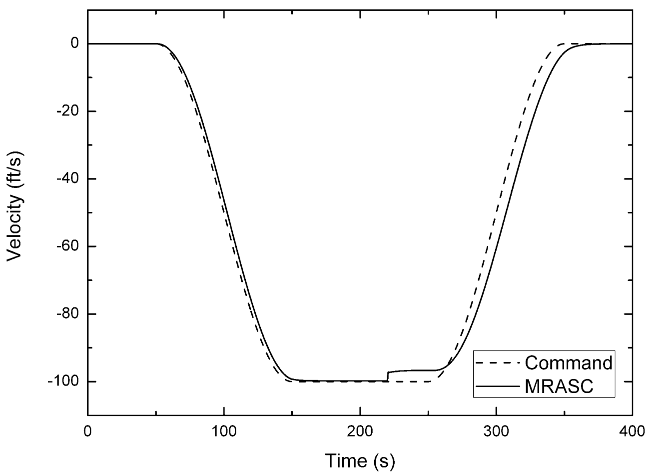

Fig. 19 Trajectory of the flight velocity under the MRASC scheme for Case 2

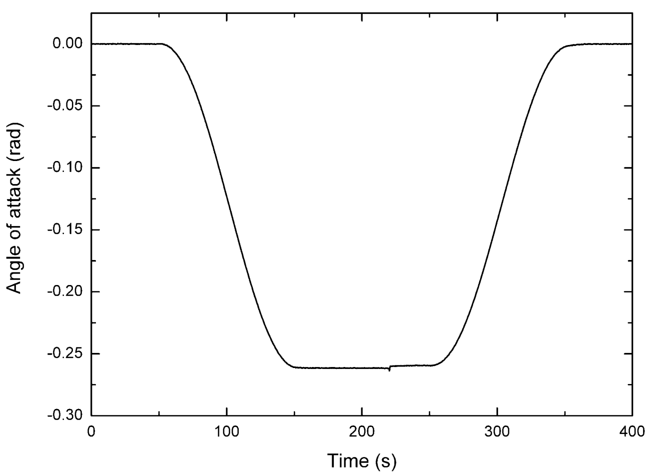

Fig. 20 Trajectory of the angle of attack under the MRASC scheme for Case 2

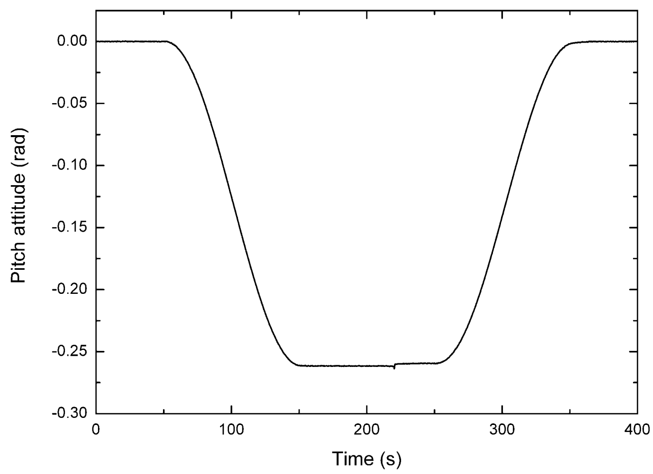

Fig. 21 Trajectory of the pitch attitude under the MRASC scheme for Case 2

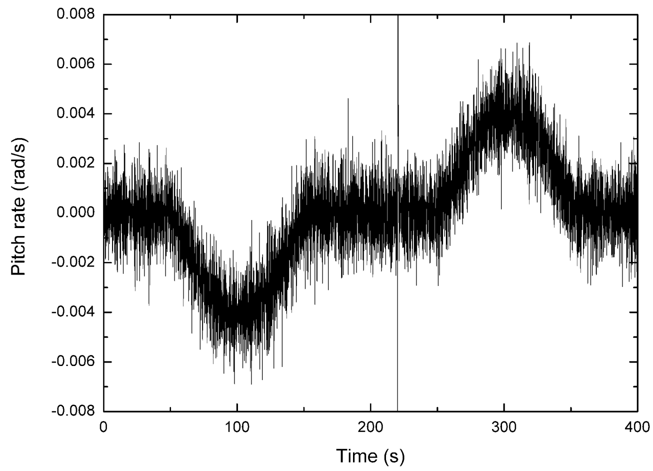

Fig. 22 Trajectory of the pitch rate under the MRASC scheme for Case 2

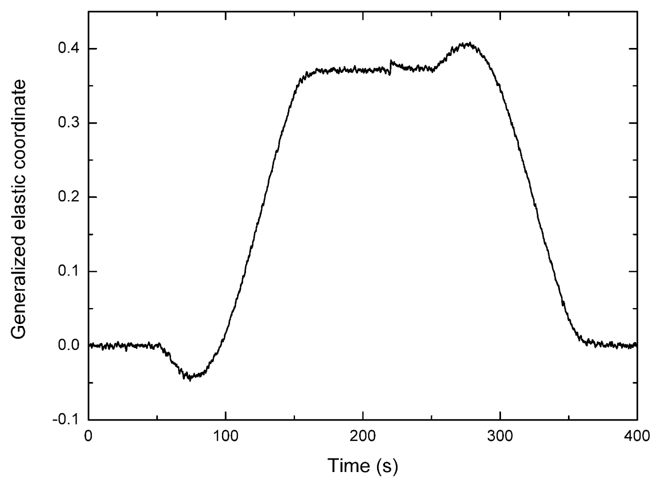

Fig. 23 Trajectory of the generalized elastic coordinate under the MRASC scheme for Case 2

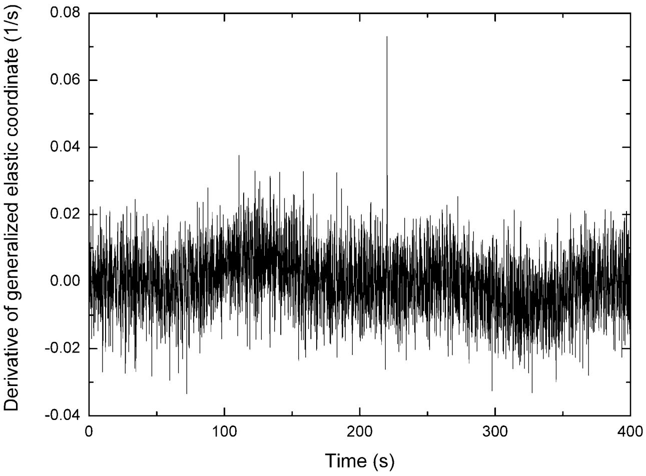

Fig. 24 Trajectory of the derivate of the generalized elastic coordinate under the MRASC scheme for Case 2

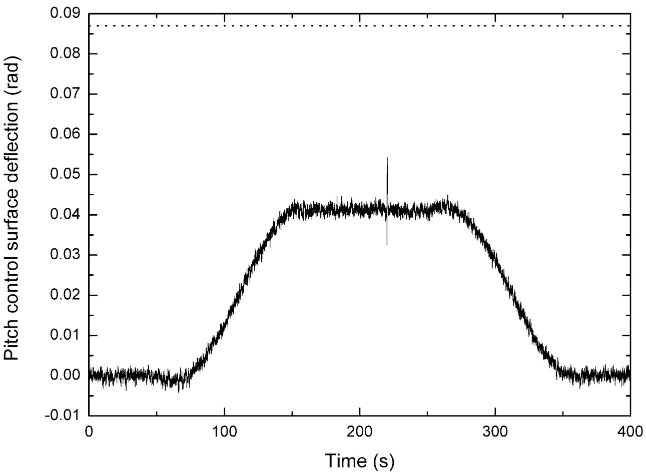

Fig. 25 Trajectory of the pitch control surface deflection under the MRASC scheme for Case 2 (note dotted line: upper bound of 0.087 rad)

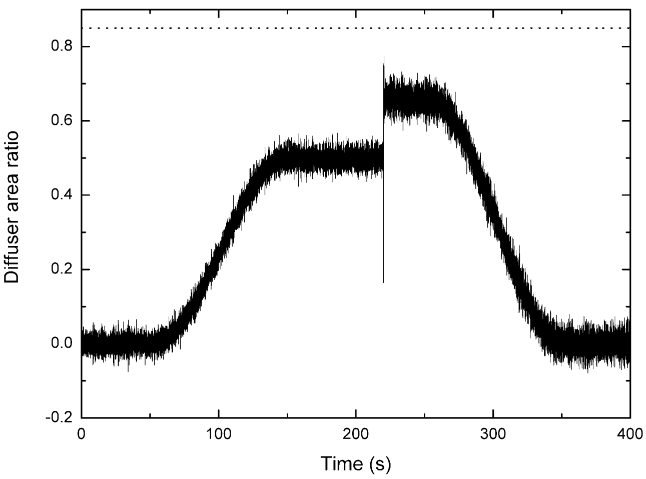

Fig. 26 Trajectory of the diffuser area ratio under the MRASC scheme for Case 2 (note dotted line: upper bound of 0.85)

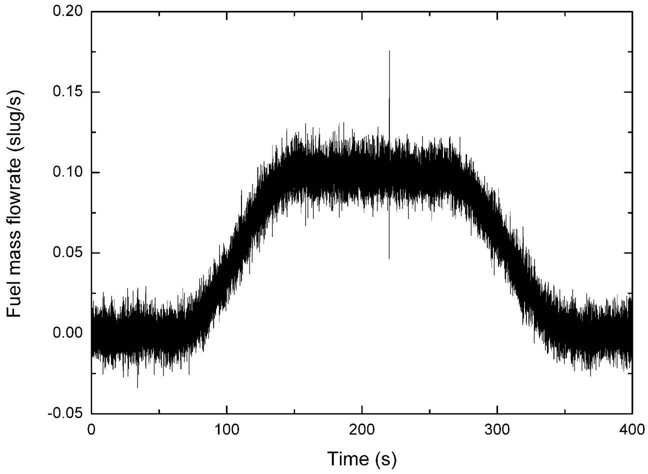

Fig. 27 Trajectory of the fuel mass flowrate under the MRASC scheme for Case 2

anti-windup approaches, the proposed scheme can ensure globally asymptotical stability for uncertain unstable plants. Moreover, compared with direct approaches, less conservative results can be achieved. Furthermore, the MRASC system is proved to be globally asymptotically stable provided that a set of LMIs holds. Simulation results show the effectiveness of the proposed control scheme. Future work will include the inclusion of a gradual expansion of the flight envelope, and investigate the qualitative behaviour of the control scheme, especially the performance when the system encounters large disturbances or possible frequent switching actions.

ACKNOWLEDGEMENTS

The authors would like to thank the reviewers for their valuable suggestions on how to clarify the analysis and improve the readability of the paper. This work was supported by the Aviation Science Foundation of China (20080151002), the Aviation Science and Technology Foundation of China (08C51011), and the National Natural Science Foundation of China (60974014).

REFERENCES

1 **Fidan, B., Mirmirani, M.,** and **Ioannou, P. A.** Flight dynamics and control of air-breathing hypersonic vehicles: review and new directions. AIAA paper 2003-7081, 2003.

2 **Mooij, E.** Numerical investigation of model reference adaptive control for hypersonic aircraft. *J. Guid., Control Dyn.*, 2001, **24**(2), 315–323.

3 **Wei, J., Yu, Y.,** and **Jie, Y.** Research on robust control of hypersonic vehicle. *J. Astronaut.*, 2008, **29**(5), 1526–1530.

4 **Gregory, I. M., Chowdhry, R. S., McMinn, J. D.,** and **Shaughnessy, J. D.** Hypersonic vehicle model and control law development using H_∞ and μ-synthesis, report no. TM-4562, NASA, Langley Research Center, 1994.

5 **Corradini, M. L.** and **Orlando, G.** Linear unstable plants with saturating actuators: robust stabilization by a time varying sliding surface. *Automatica*, 2007, **43**(1), 88–94.

6 **Sajjadi-Kia, J. F.** Combing anti-windup and over-saturation. AIAA paper 2007-6401, 2007.

7 **Landau, I. D.** *Adaptive control: the model reference approach*, 1979 (Marcel Dekker, New York, NY).

8 **Zhao, J.** and **Hill, D. J.** Dissipativity theory for switched systems. *IEEE Trans. Autom. Control*, 2008, **53**(4), 941–953.

9 **Shorten, R. N., Wirth, F., Mason, O., Wulff, K.,** and **King, C.** Stability theory for switched and hybrid systems. *SIAM Rev.*, 2007, **49**(4), 545–592.

10 **Haddad, W. M.** and **Bernstein, D. S.** Explicit construction of quadratic Lyapunov functions for the small gain, positivity, circle, and Popov theorems and their application to robust stability, part I: continuous-time theory. *Int. J. Robust Nonlinear Control*, 1993, **3**, 313–339.

11 *Aviation Week & Space Technology*, 29 October 1990, p. 46.

12 **Chavez, F. R.** and **Schmidt, D. K.** Uncertainty modeling for multivariable control robustness analysis of elastic high speed vehicles. *J. Guid., Control Dyn.*, 1999, **22**(1), 87–95.

13 **Mooij, E.** Model reference adaptive guidance for re-entry trajectory tracking. AIAA paper 2004-4775, 2004.

14 **Erzberger, H.** Analysis and design of model following systems by state space techniques. In Proceedings of the Joint Conference on *Automatic control*, Ann Arbor, Michigan, June 1968, pp. 572–581.

15 **Zhang, H. Y.** and **Wang, Q.** *Optimal control theory and applications*, 2006 (Higher Education Publishing, Beijing, China).

16 **Buschek, H.** *Synthesis of fixed order controllers with robustness to mixed real/complex uncertainties*. PhD Thesis, School of Aerospace Engineering, Georgia Institute of Technology, 1995.

17 **Justus, C. G., Campbell, C. W., Doubleday, M. K.,** and **Johnson, D. L.** New atmospheric turbulence model for shuttle applications, report no. TM-4168, NASA, George C. Marshall Space Flight Center, 1990.